AD-A055 384 MASSACHUSETTS INST OF TECH CAMBRIDGE AEROPHYSICS LAB F/G 20/4
PRELIMINARY EXPERIMENT DESIGNED TO SUPPORT A FEASIBILITY DEMONS--ETC(U)
APR 78 E E COVERT, A R KANEVSKY F49620-77-C-0031
UNCLASSIFIED MIT-TR-202 AFOSR-TR-78-0902 NL

1 OF 1
AD A055 384

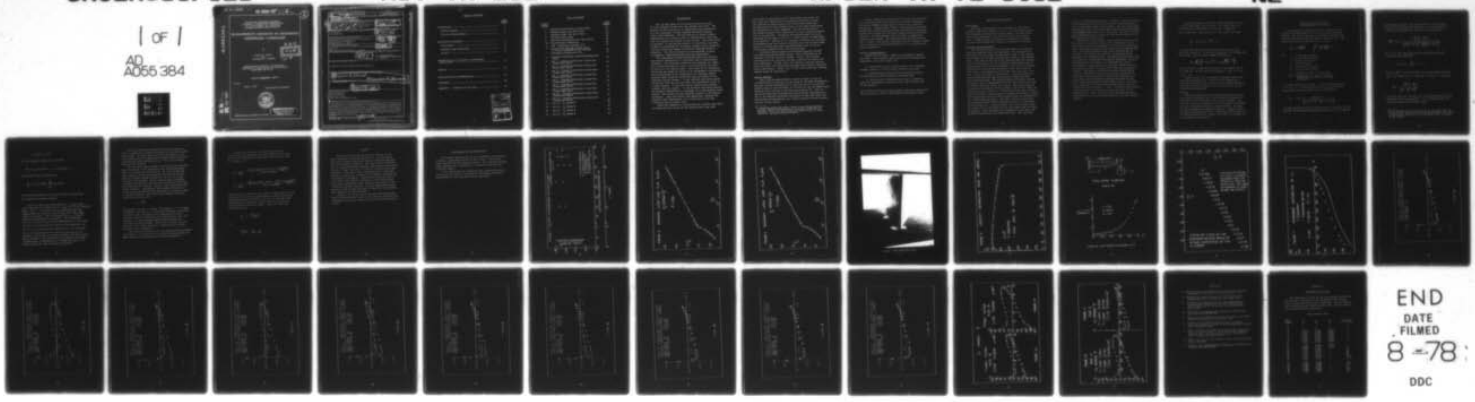

END
DATE FILMED
8-78
DDC

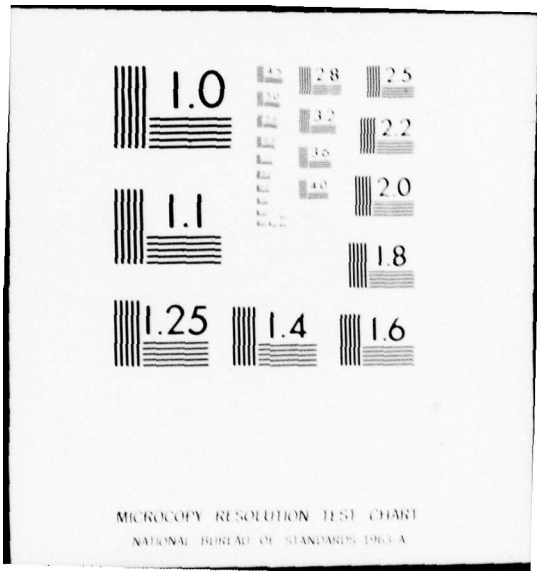
1.0
1.1
1.25
1.4
1.6
2.8
2.5
3.2
2.2
3.6
2.0
4.0
1.8
MICROCOPY RESOLUTION TEST CHART
NATIONAL BUREAU OF STANDARDS 1963-A

(2)

Preliminary Experiment Designed to Support a Feasibility Demonstration of a Novel Method for Developing Unsteady Boundary Layer Profiles

MASSACHUSETTS INSTITUTE OF TECHNOLOGY
AEROPHYSICS LABORATORY

by

Eugene E. Covert
and
Alexander R. Kanevsky

Massachusetts Institute of Technology
Department of Aeronautics and Astronautics
Cambridge, Ma 02139

Interim ~~Scientific~~ Report

TR 202

April, 1978

Distribution Unlimited

AFOSR Contract F49620-77-C-0031

UNCLASSIFIED

SECURITY CLASSIFICATION OF THIS PAGE (When Data Entered)

REPORT DOCUMENTATION PAGE	READ INSTRUCTIONS BEFORE COMPLETING FORM
1. REPORT NUMBER: AFOSR-TR-78-0902	2. GOVT ACCESSION NO. / 3. RECIPIENT'S CATALOG NUMBER
4. TITLE (and Subtitle): PRELIMINARY EXPERIMENT DESIGNED TO SUPPORT A FEASIBILITY DEMONSTRATION OF A NOVEL METHOD FOR DEVELOPING UNSTEADY BOUNDARY LAYER PROFILES	5. TYPE OF REPORT & PERIOD COVERED: INTERIM rept. 1 Jan 77 - 31 Dec 77
	6. PERFORMING ORG. REPORT NUMBER: MIT TR 202
7. AUTHOR(s): E E COVERT, A R KANEVSKY	8. CONTRACT OR GRANT NUMBER(s): F49620-77-C-0031
9. PERFORMING ORGANIZATION NAME AND ADDRESS: MASSACHUSETTS INSTITUTE OF TECHNOLOGY, AEROPHYSICS LABORATORY, CAMBRIDGE, MA 02139	10. PROGRAM ELEMENT, PROJECT, TASK AREA & WORK UNIT NUMBERS: 2307A2, 61102F, A2
11. CONTROLLING OFFICE NAME AND ADDRESS: AIR FORCE OFFICE OF SCIENTIFIC RESEARCH/NA, BLDG 410, BOLLING AIR FORCE BASE, D C 20332	12. REPORT DATE: April 1978
	13. NUMBER OF PAGES: 37
14. MONITORING AGENCY NAME & ADDRESS (if different from Controlling Office): 39 p.	15. SECURITY CLASS. (of this report): UNCLASSIFIED
	15a. DECLASSIFICATION/DOWNGRADING SCHEDULE

16. DISTRIBUTION STATEMENT (of this Report)

Approved for public release; distribution unlimited.

17. DISTRIBUTION STATEMENT (of the abstract entered in Block 20, if different from Report)

Eugene E. Covert
Alexander R. Kanevsky

18. SUPPLEMENTARY NOTES

MIT-TR-202

19. KEY WORDS (Continue on reverse side if necessary and identify by block number)

GROUND TESTING
WIND TUNNELS
UNSTEADY FLOW
UNSTEADY BOUNDARY LAYER

20. ABSTRACT (Continue on reverse side if necessary and identify by block number)

The feasibility of a new experimental technique for studying the effect of unsteady flows on boundary layers is under development. The method studied uses a stationary NACA 0012 airfoil in a steady subsonic wind tunnel. Unsteadiness in the flow over the airfoil would be generated by an unsteady external aerodynamic interference. Initial results are reported in which upwash effects of stationary cylinders of several sizes located at different positions downstream and below the airfoil are measured. The position for ~~minimum~~ maximum influence is determined.

009 2.00

DD FORM 1 JAN 73 1473 EDITION OF 1 NOV 65 IS OBSOLETE

UNCLASSIFIED

SECURITY CLASSIFICATION OF THIS PAGE (When Data Entered)

Table of Contents

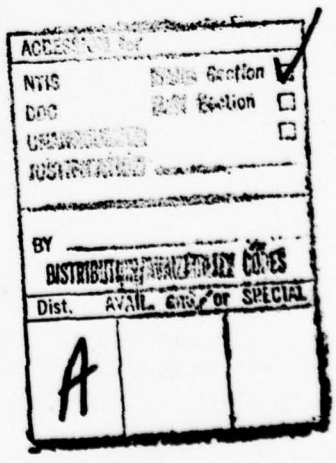

List of Figures

Introduction

This is the report of activities carried out under Contract F49620-77-C-0031 for the calendar year 1977. The purpose of this contract is to demonstrate the feasibility of a new technique to study unsteady turbulent boundary layers experimentally. The difficulties of making careful measurements on a moving airfoil or generating an airstream that is unsteady and uniform are well known. The former leads to problems of driving the airfoil, of extracting the data, as well as correcting for transducer reading errors caused by inertial loads which appear as spurious unsteady forces or pressures. The latter presents its own problems of power consumption, complicated geometries and installation.

The experimental studies performed under this contract demonstrate feasibility of a different type of experimental technique. The principle underlying the technique is simple. The circulation about an airfoil is controlled by the angle of attack at its trailing edge. This angle can be changed by distorting the shape of airfoil or by aerodynamic interference. This interference is the consequence of a suitably shaped external body located to change the angle of attack or the effective airfoil chamber. If the external body moves nearer and further from the trailing edge, the circulation varies in a known fashion. In this way one can control the pressure gradient over the airfoil. If the external body moves quickly, the pressure distribution is unsteady, as is the boundary layer. However, the airfoil and the measuring surface is and remains stationary. Thus with proper instrumentation, pressure and boundary layer measurements can be made with little more difficulty than in steady flow.

Since the technique of controlling the trailing edge angle of attack had not, as far as the authors know, been used

previously in the present form*, the primary activities for the first year consisted of experiments designed to support the validity of the procedure and to partially define the characteristics of the boundary layer in the wind tunnel where the experiment is to be conducted. For the initial effort, the steady boundary layer properties in a zero pressure gradient were to be measured. Ultimately the boundary layer is to be developed on the upper surface of a fixed airfoil, an NACA 0012, to be specific. Because it is necessary to measure the pressure distribution over the airfoil, including near the trailing edge, there is a possibility that some approximate data on the unsteady Kutta condition will also be generated.

Ultimately these studies could provide detailed information about unsteady boundary layers. This information is of technical interest for three reasons. First, the unsteady characteristics of turbulent boundary layers do not seem to be well understood. Second, there are numerous technical applications for which the information developed could lead to improved device performance. Third, data of this kind could help validate results found by computation.

General Remarks

Even a disinterested observer would be able to note an increased level of activity in the study of unsteady aerodynamics. The most obvious manifestation of this interest is in both the AFOSR meeting at the University of Arizona (1) and the AGARD Fluid Dynamics Panel meeting on Unsteady Aerodynamics (2). This interest may have been stimulated because unsteady aerodynamics is one of the physical processes that govern or may even limit the performance of helicopters, gas turbine engines and wind turbines used as a power source.

---

*It should be noted that A.M.O. Smith in his Wright Brothers Lecture "High-Lift Aerodynamics" (reported in Journal of Aircraft, 1975) used this technique theoretically to study high-lift, multiple element airfoils.

Another reason for the increased interest may stem from the realization that many aspects of unsteady aerodynamics may now be studied through uses of large scale automatic computation. Computational study is particularly attractive because the difficulties which limit analytical or classical experimental studies do not limit studies carried out by the computer. The experimental data is useful in supporting computational studies. The synergysm that results from the use of results from theory, experiment and the computer cannot fail to lead to a fuller understanding of a particular aerodynamic phenomenon.

Current Accomplishments

During the last year a number of preliminary studies were made. These studies, which constituted necessary prerequisites to the main study, are:

1. Measurement of the characteristics of a turbulent boundary layer on a zero pressure gradient flat plate.

2. Verification of the ability to measure pressure distribution on an 0012 airfoil in uniform flow.

3. Verification of the ability to vary circulation using the aerodynamic interference near the trailing edge of the airfoil.

The results from each of these studies, which are abstracted from Reference 3, will be discussed in more detail below.

Experimental Equipment

Wind Tunnel

All tests reported here were conducted in the Wright Brothers Wind Tunnel (WBWT) at M.I.T. It is a closed return facility with a 10 foot (3.05 meter) wide, 7.15 foot (2.29 meter) high elliptical test section 15 feet (4.57 meter) long. A 2000 HP motor provides wind speed up to 140 miles per hour (62.5 meters per second) at atmospheric pressure.

Boundary Layer Experiment

The two-dimensional flat plate provided the surface on which the boundary layer was developed. The dimensions of the plate were 36 inches (0.9144 meter) long, 1 inch (0.0254 meter) thick and 20 inches (0.5080 meter) wide at the leading edge. The width of the gap at its trailing edge was slightly larger to compensate for the streamline displacement due to the boundary layers on the end plates. The use of end plates helped insure the two-dimensionality of the flow over the flat plate. The dimensions of the end plates were 60 x 75 x 1 in. (1.5240 x 1.9050 x 0.0254 meter). The end plates had three static pressure taps and the plate itself had five static pressure taps. The leading edge of the plate started 10 inches (.254 m) downstream of the 48 inch (121.9 m) strips of plywood that made up the side walls. The leading edge of the strip was beveled from the outside at 15^{o} with a radius of roughly 1/8 inch (0.0032 m). The bottom of the plate leading edge was roughly a tangent ogive of radius 50.5 inches (1.282 m). The tangent point was 10 inches (2.54 m) from the leading edge. The leading edge was sharp. The upper surface of the plate was Blanchard ground and was smooth to within 35 microinches (8.98 micrometers). Static pressure taps were located along the center line of the plate and off the center line, as shown in Figure 2. The end plates were angulated in yaw until the pressure distribution was essentially flat. The resulting

gaps were sealed with plasticine. Figure 2 shows the velocity distribution along the top of the plate, normalized with respect to the wind tunnel "speed holes". The two cases shown correspond to the final pitch angle setting, with and without the boundary layer probe drive mechanism. The axial velocity ratio was relatively constant over the last 8 inches (.2 m) of the plate at 1.060 ± .002.

The velocity distribution in the boundary layer on the flat plate was measured using a Flow Corporation series 900 hotwire anemometer operated in the constant temperature mode. The active element of the system was a platinum wire 1 in. (2.54 cm) long and 0.0005 inches (0.01272 mm) in diameter. The hotwire was held by a cylindrical probe attached to a streamlined arm. A probe drive mechanism with two degrees of freedom was attached to the plate. Vertical displacement of the hotwire, as indicated by a linear potentiometer, was measured by a digital voltmeter and was recorded on a Hewlett-Packard model 3400A two-dimensional plotter. The hotwire anemometer had been calibrated by using the relationship between the output voltage of the linearizer and the velocity of free stream measured by a pitot tube. The calibration constant was found for the probe positioned outside of the boundary layer. The probe drive mechanism and calibration constant were used to determine the local velocity $u(y)$. A standard pitot-static probe was also used to measure local velocities in the boundary layer. When corrected using the Young and Mass displacement effect, the two methods give the same velocity profile.

Typical velocity profiles are shown in Figures 2 and 3 in the form of the inner variable. For these curves u_τ is based upon Schlicting's results ($C_f = .0034$) at $Re_\theta \sim 6{,}500$ (4). This leads to an inner law of the form

$$\frac{u}{u_\tau} = 5.75 \log_{10} \frac{yu_\tau}{\nu} + 5.5$$

in good agreement with the constants given in Duncan, Thom and Young (5). By use of the suggestion of Clauser (6) who writes; using the free stream velocity, v_∞

$$\frac{u}{v_\infty} = \sqrt{\frac{2}{C_f}} \left\{ A \left(\log_{10} \frac{yv_\infty}{\nu} + \log_{10} \sqrt{\frac{C_f}{2}} \right) + B \right\}$$

one can iterate graphically to obtain a consistent fit of A, B and C_f. In this way we obtained $C_f = .003$, $A = 5.75$ and $B = 5.1$.

These results are in reasonable agreement with those reported by Fernholz (7). These results suggest the turbulent boundary layers generated in the Wright Brothers Wind Tunnel will be adequate for the purposes of the experimental work planned.

Airfoil

The 0012 airfoil was based upon coordinates given by Abott and von Doenhoff (8). The airfoil was machined in two halves, with 19 pressure taps on each surface. The pressure taps were connected to a Setra pressure transducer through a Scannivalve pressure scanning value. The wing and its end plates are shown in Figure 4. Figure 5 shows the 0012 airfoil develops local velocities within about ± 1% of those given by Abott. Hence, the airfoil is assumed to be adequate for these tests.

Demonstration of Principle of Aerodynamic Interference

For purposes of analysis the usual assumptions of linearized aerodynamics of an incompressible fluid were adopted. The local tangential perturbation velocity can be computed from the integral given in Thwaites (9). The origin is located at the nose of the airfoil.

$$\frac{u}{V_\infty} = \pm \frac{1}{\pi}\sqrt{\frac{c-x}{x}} \int_0^c \frac{\alpha(\xi)}{x-\xi}\sqrt{\frac{\xi}{c-\xi}}\, d\xi$$

here
- $+$ is the upper surface
- $-$ is the lower surface
- x station of interest
- c airfoil chord
- u perturbation velocity
- V_∞ free stream velocity
- ξ running variable of integration
- $\alpha(x)$ distribution of angle of attack or camber over the airfoil, measured in radians

A circular cylinder of radius a with center located at $x = \ell$ and $z = -z'$ (Figure 6a) causes an angle of attack distribution along the chord line of the airfoil.

$$\alpha(x) = \tan^{-1} \frac{2a^2 (\ell-x) z'}{\left[(\ell-x)^2+z'^2\right]^2 - a^2\left[(\ell-x)^2-z'^2\right]}$$

For each distance from the trailing edge to the center of the cylinder the maximum induced angle of attack at the trailing

edge can be computed. The locus position of the center of the circle is shown in Figure 6b. It is convenient to normalize all lengths with respect to the chord; i.e.,

$$\alpha\left(\frac{x}{c}\right) = \tan^{-1} \frac{2\,\frac{a^2}{c^2}\left(\frac{\ell}{c} - \frac{x}{c}\right)\frac{z'}{z}}{\left[\left(\frac{\ell}{c}-\frac{x}{c}\right)^2+\left(\frac{z'}{c}\right)^2\right]^2 - \frac{a^2}{c^2}\left[\left(\frac{\ell}{c}-\frac{x}{c}\right)^2-\left(\frac{z'}{c}\right)^2\right]}$$

If $\alpha < 8^{o}$, this expression can be simplified using the linearizing approximation

$$\tan^{-1} y \pm y + \frac{y^3}{3} + \ldots \simeq y$$

The term $\left(\frac{a}{c}\right)^2$ in the denominator is neglibly small for this case. For simplicity, we denote $\frac{z'}{c} = \bar{h}$ and $\frac{\ell}{c} = \bar{\ell}$, finally:

$$\alpha\left(\frac{x}{c}\right) \simeq \frac{2\,\frac{a^2}{c^2}\left(\bar{\ell} - \frac{x}{c}\right)\bar{h}}{\left[\left(\bar{\ell} - \frac{x}{c}\right)^2 + \bar{h}^2\right]^2}$$

This expression for the angle of attack distribution is then substituted into the integral.* It is evaluated most conveniently through the variable change

*For the purpose of this calculation, we are neglecting the effect of the airfoil in flow over the cylinder. The error so incurred is not large if the cylinder is not too close to the airfoil.

$$x = \frac{c}{2} (1 + \cos \theta)$$

and the assumption that on the airfoil

$$\alpha(\theta) = B_o + B_1 \cos \theta + \ldots + B_n \cos n\theta + \ldots$$

from which it may be deduced (9)

$$\frac{u}{v_\infty} = \pm \; B_o \tan \frac{\theta}{2} + \sum_{n=1}^{\infty} B_n \sin n\theta$$

The term B_o represents the constant angle of attack and B_n represents curvature effects.

Figure 6c shows the distribution of α due to the 0.125" cylinder so located that $\alpha = \alpha_{max} = 8^o$ at the trailing edge. Note α is largest near the trailing edge, the average angle of attack is fairly small, but some camber effect is apparent. The distribution of c_p is compared with the measured value in Figure 7. The difference between the measured c_p and the calculated c_p, on the upper surface is partly due to the inaccuracy introduced by the $\tan \frac{\theta}{2}$ term, which becomes singular at $\bar{x} = 0$, and partly due to the separation of the flow over the back of the cylinder. The effect of cylinder diameter was tested using three cylinders. The cylinders had a length of 20 inches (0.5080 meter) and diameters of 5 inches (0.1270 m), 2.5 inches (0.0635 m), and 1.25 inches (0.0318 m).

Having verified the principle that this procedure is valid, a design for a support mechanism to move the cylinder was started. It turned out the primary structure in the wind tunnel would not support the needed dynamic loads that arose at high speed cylinder motion. Thus, an alternate procedure was studied.

One can agree that the angle of attack at the trailing edge is related to the curvature of the interfering body. Thus, if one made an elliptic body, one could change the local angle of attack and camber by rotating the ellipse. This is a simpler dynamic problem by far, as far as the structure is concerned. The rotating ellipse introduces a complication that the spinning may introduce circulation about the axis of rotation. However, this additional angle can be measured. Fortunately, the potential flow past a circle can be transformed into flow past an ellipse through a conformal mapping. The ellipse was designed using the conformal transformation

$$\zeta = z + \frac{k^2}{z}$$

The circle is in the z plane, its radius $r = \ell = 2$ inches (0.0508 m). We chose $k = 1.25$ inches (0.0318 m) to provide an ellipse whose semi-major axis simulated the 5 inch cylinder and whose semi-minor axis simulated the 1.25 inch cylinder. In the spanwise direction the ellipse had 20 inches (0.509 m) length. The ellipse could be rotated about the axis, while rotating it simulated the smallest and the largest cylinders.

The ellipse was fixed to the end plates below and behind the airfoil. The details of the several configurations for which measurements were made are given in Appendix A.

The pressure data was converted into pressure coefficients for the upper and lower halves of the wing. The pressure transducer calibration relations were used to find c_p; i.e.

$$c_{p\ \substack{\text{loc.}\\ \text{upper}}} = \frac{\text{output upper volts} \times 6.7\ \frac{\text{in. alcohol}}{\text{volts}}}{\Delta h \text{ in. alcohol}}$$

$$c_{p\ \substack{\text{loc.}\\ \text{upper}}} = \frac{\left[(\text{output lower volts}) - A\right] 6.7\ \frac{\text{in. alcohol}}{\text{volts}}}{\Delta h \text{ in. alcohol}}$$

These plots were made for the airfoil aligned with the free stream and for different wing-cylinder combinations which changed the angles of attack. On most of the plots the distribution of the local coefficients of pressure was plotted versus percent of chord. Using the following definition of c_p

$$c_p = 1 - \left(\frac{u_{local}}{v_\infty}\right)^2$$

or

$$\frac{u_{local}}{v_\infty} = \sqrt{1 - c_p}$$

Results

Figures 8-21 show the pressure coefficient on the upper and lower surface of the airfoil. Figure 8 shows the airfoil alone; inserting a quarter chord cylinder has the effect shown in Figure 9. Here the pressure distribution is measured when the trailing edge angle is about 8-1/2 degrees. Figure 11 is for a value of 2.1 degrees for that parameter. Note the pressure distribution is relatively uniform in each case. Figures 12-14 show the same data for a cylinder of 1/8 chord. Figures 15-17 show the same result with a 1/16 diameter cylinder at the trailing edge. Since the trailing edge angle varies as the square of the normalized cylinder diameter, a direct comparison between Figures 11 and 12 show the angle of attack at the trailing edge dominates the flow process.

Finally a series of tests were made with the ellipse. Figures 18-21 show the effect of the angle of attack of the semi-major axis on the airfoil pressure coefficient distribution.

Conclusions and Recommendations

The results indicate the use of aerodynamic interference produces a predictable effect on the airfoil. This effect seems adequate for the purpose at hand. The turbulent boundary layer developed on a flat plate is consistent with that reported by others.

It is recommended that boundary layer characteristics be measured on the airfoil in steady flow and that preliminary measurements in the unsteady case be undertaken.

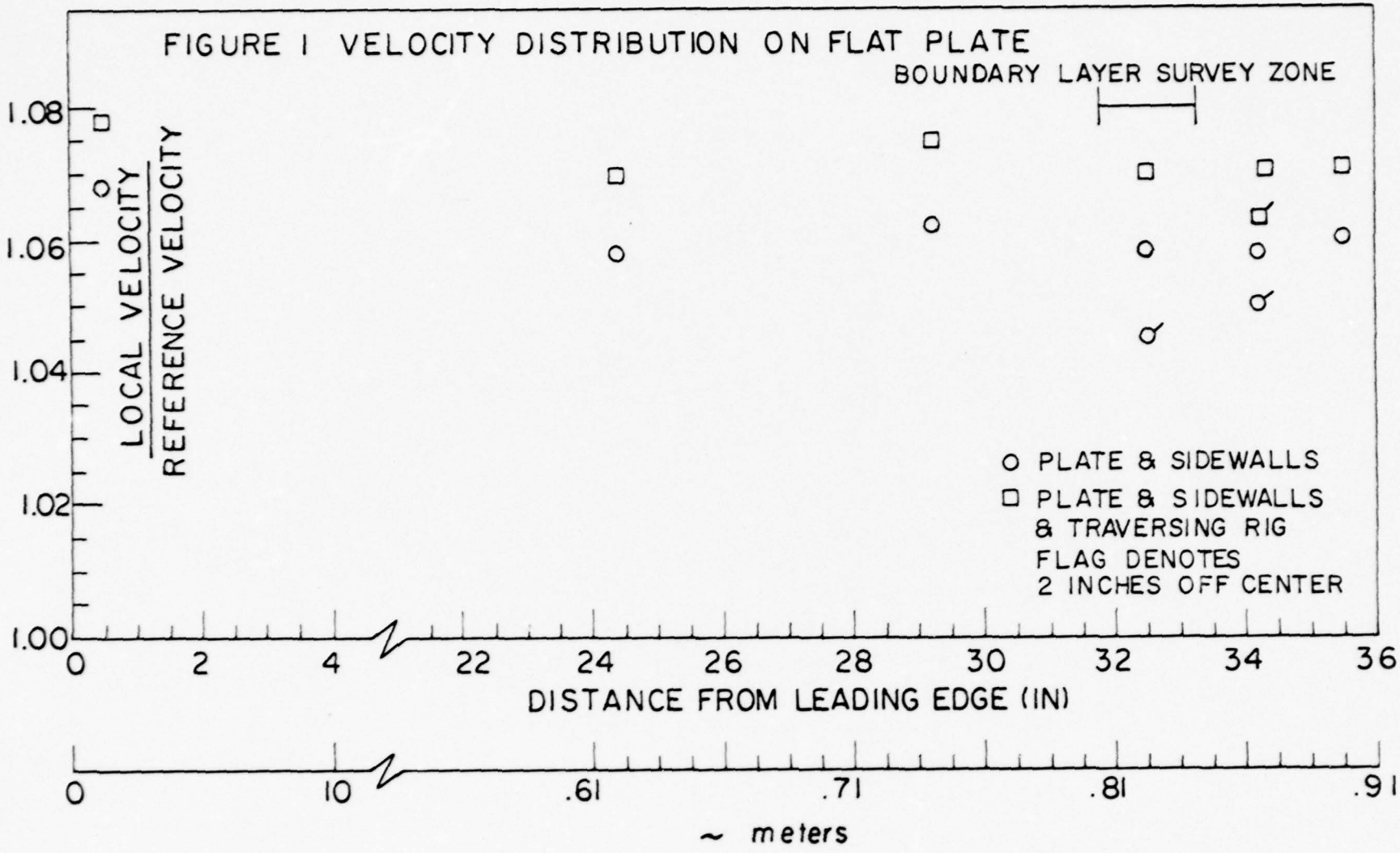
FIGURE 1 VELOCITY DISTRIBUTION ON FLAT PLATE
BOUNDARY LAYER SURVEY ZONE
LOCAL VELOCITY / REFERENCE VELOCITY
1.08
1.06
1.04
1.02
1.00
O PLATE & SIDEWALLS
□ PLATE & SIDEWALLS & TRAVERSING RIG
FLAG DENOTES 2 INCHES OFF CENTER
0
2
4
22
24
26
28
30
32
34
36
DISTANCE FROM LEADING EDGE (IN)
0
.10
.61
.71
.81
.91
~ meters

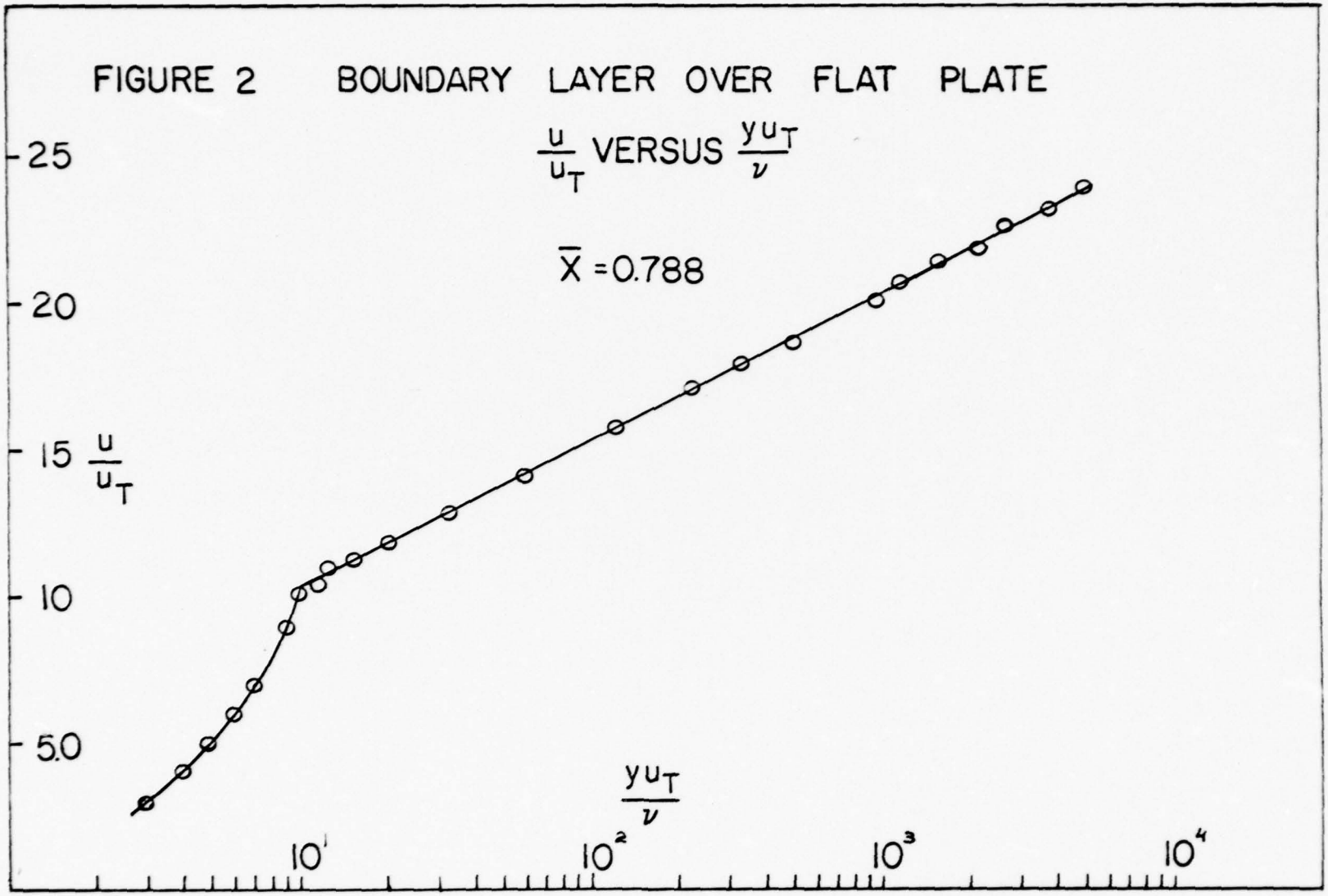
FIGURE 2 BOUNDARY LAYER OVER FLAT PLATE
$\frac{u}{u_T}$ VERSUS $\frac{y u_T}{\nu}$
$\bar{X}$ = 0.788
25
20
15 $\frac{u}{u_T}$
10
5.0
$\frac{y u_T}{\nu}$
10^1
10^2
10^3
10^4

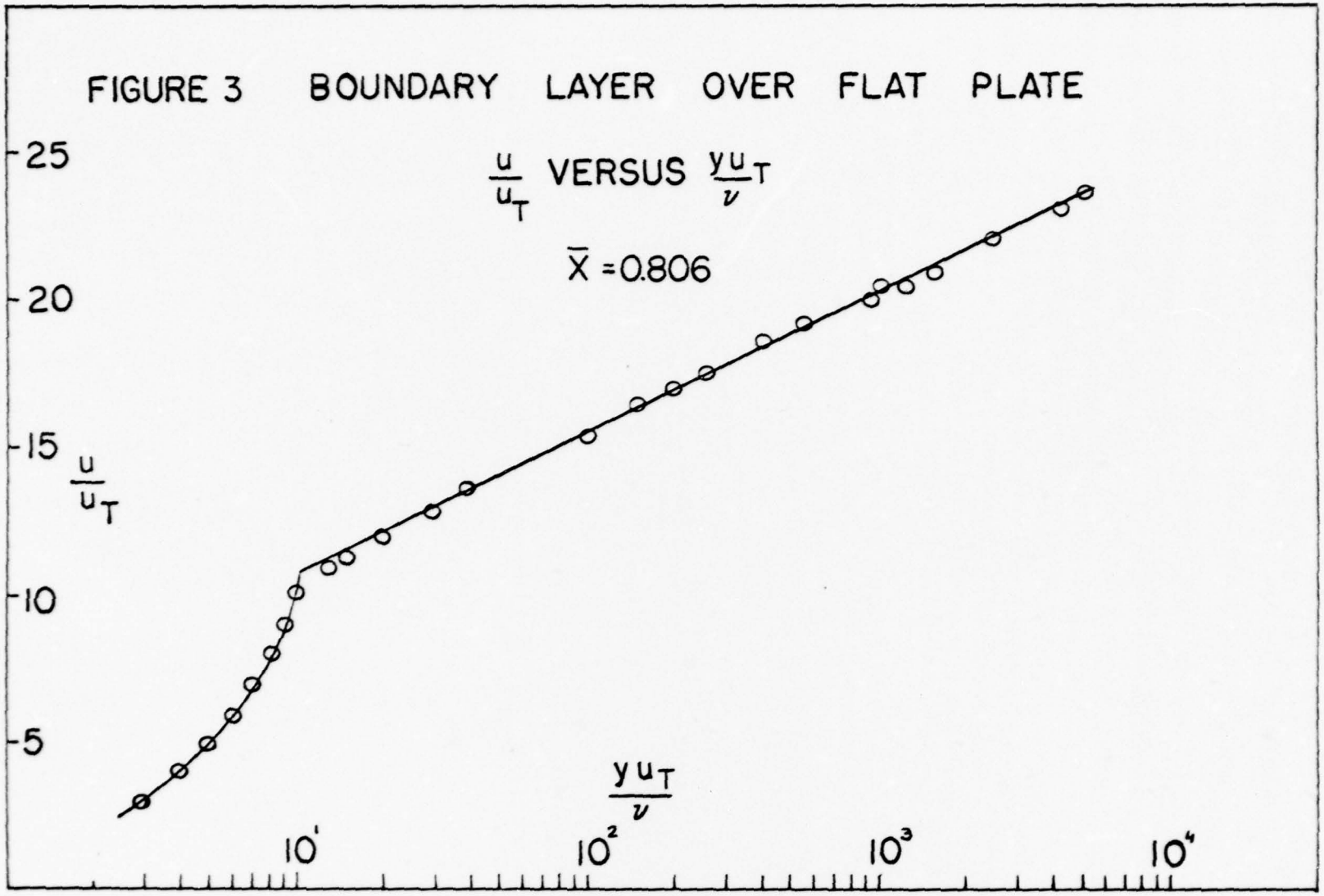
FIGURE 3 BOUNDARY LAYER OVER FLAT PLATE
$\frac{u}{u_T}$ VERSUS $\frac{y u_T}{\nu}$
$\bar{X}$ = 0.806
25
20
15
10
5
$\frac{u}{u_T}$
$\frac{y u_T}{\nu}$
10^1
10^2
10^3
10^4

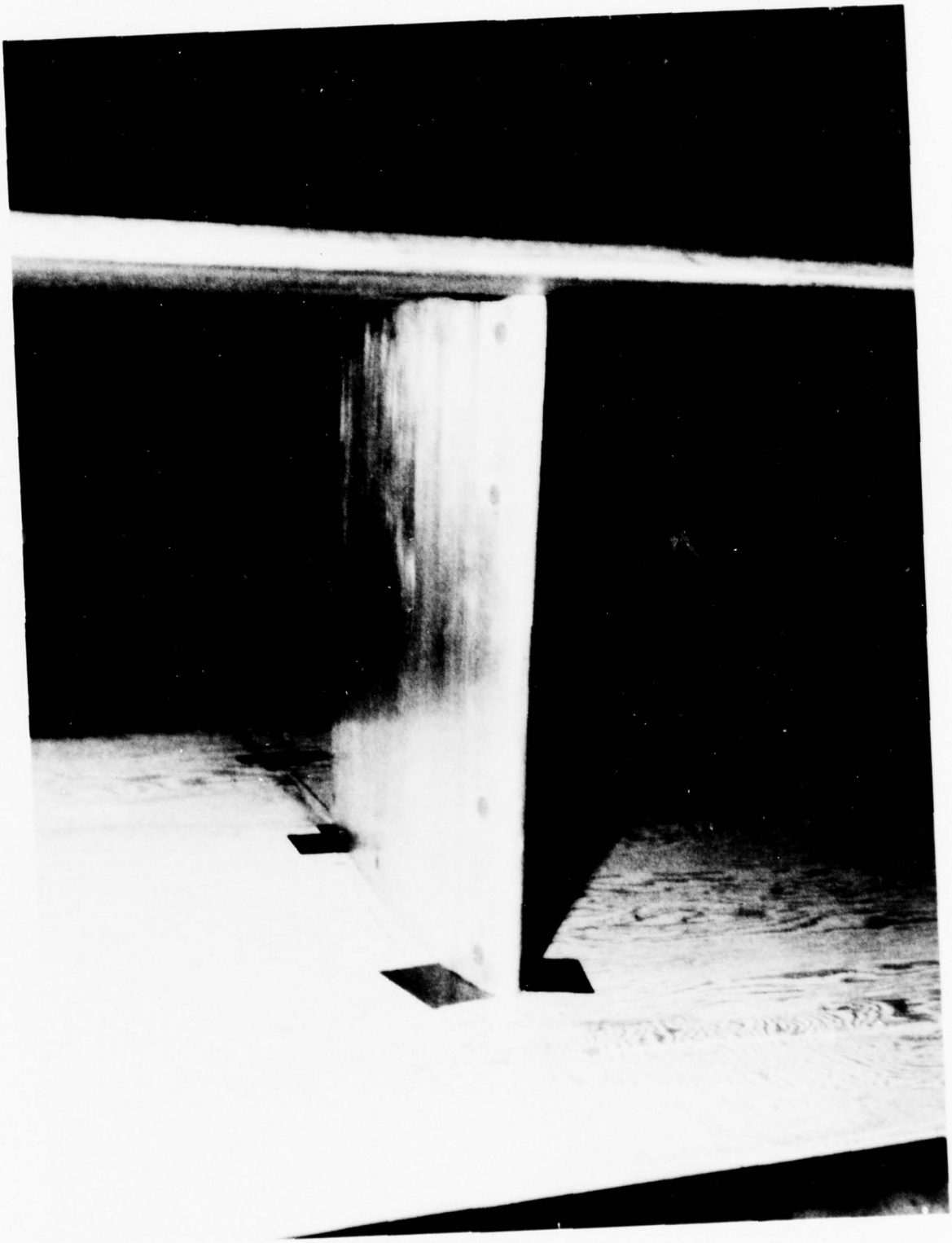

FIGURE 4 TWO-DIMENSIONAL WING

FIGURE 5 VELOCITY DISTRIBUTION OVER THE AIRFOIL

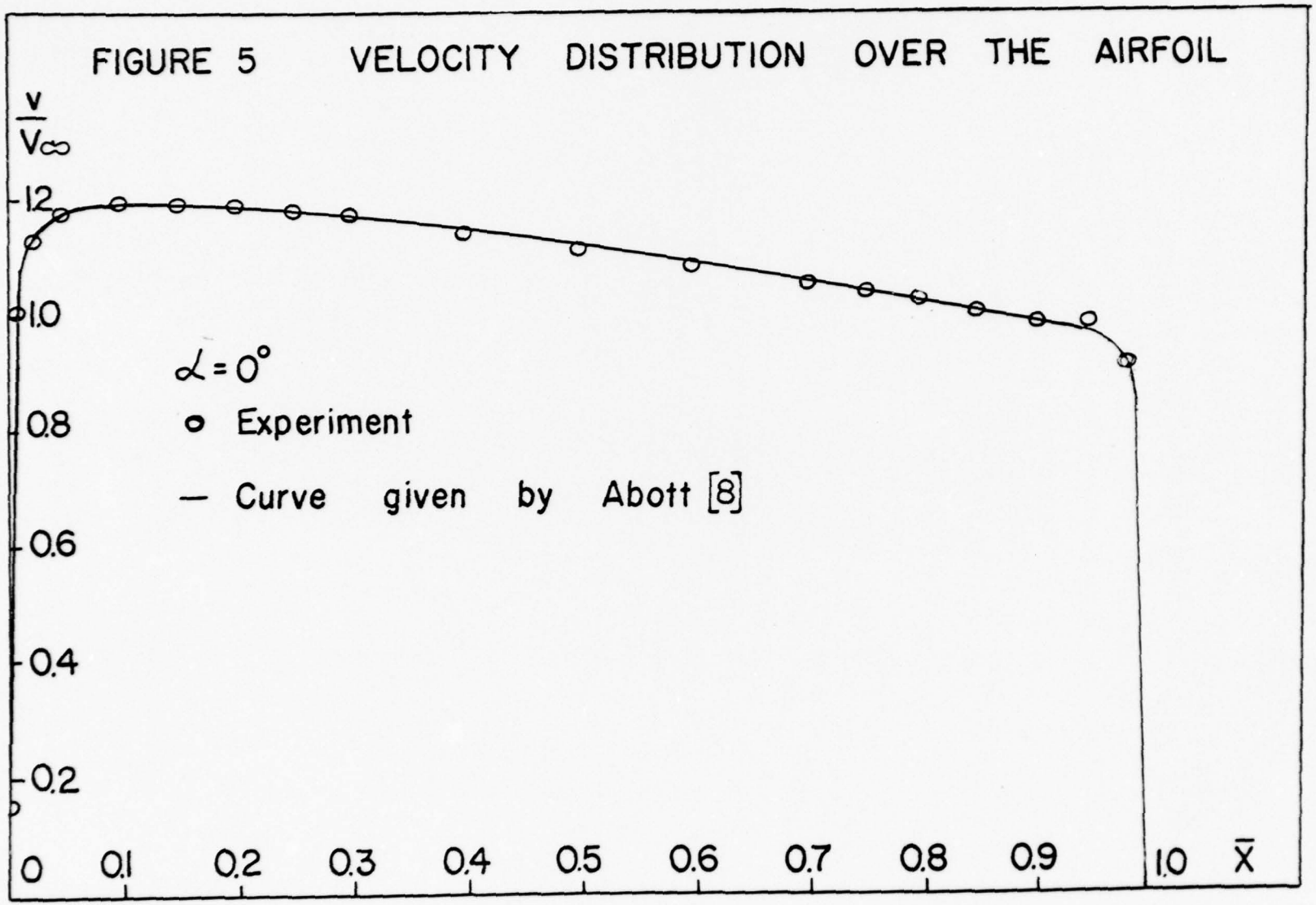

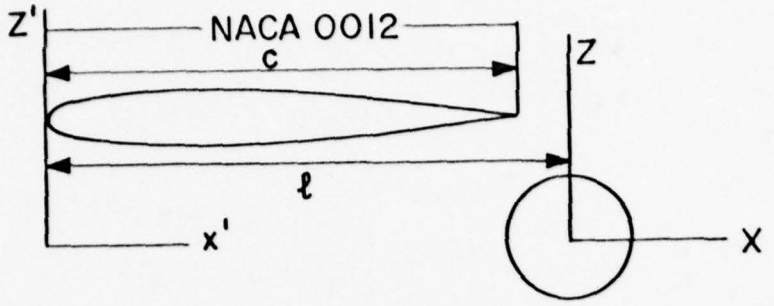

Wing - cylinder Combination

Figure 6A

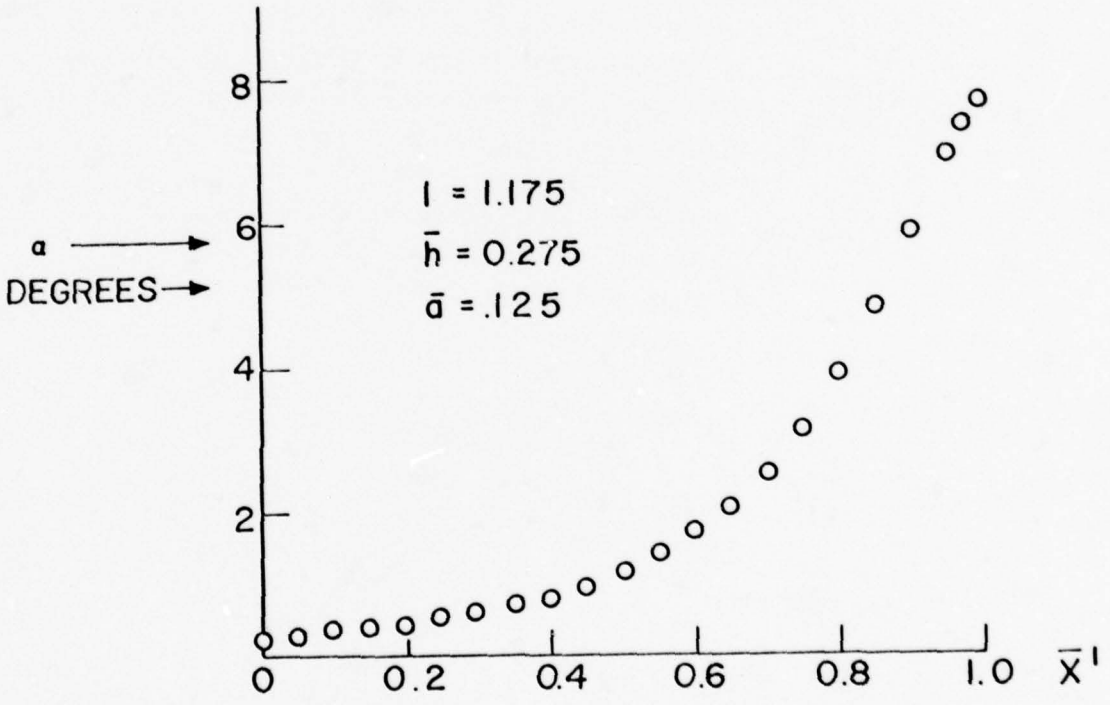

Figure 6C $\alpha(X)$ Induced by Cylinder vs $\bar{X}$

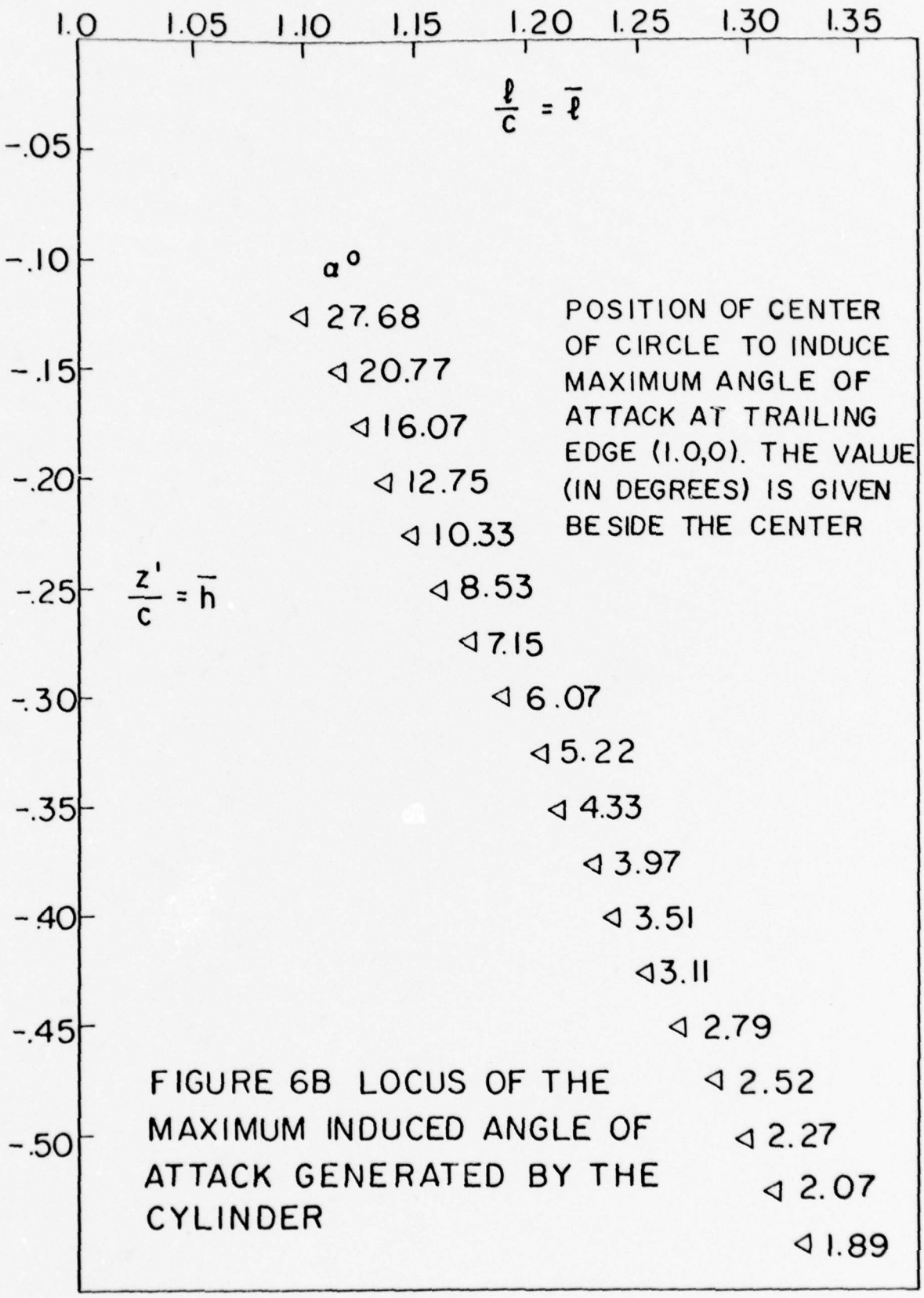

FIGURE 6B LOCUS OF THE MAXIMUM INDUCED ANGLE OF ATTACK GENERATED BY THE CYLINDER

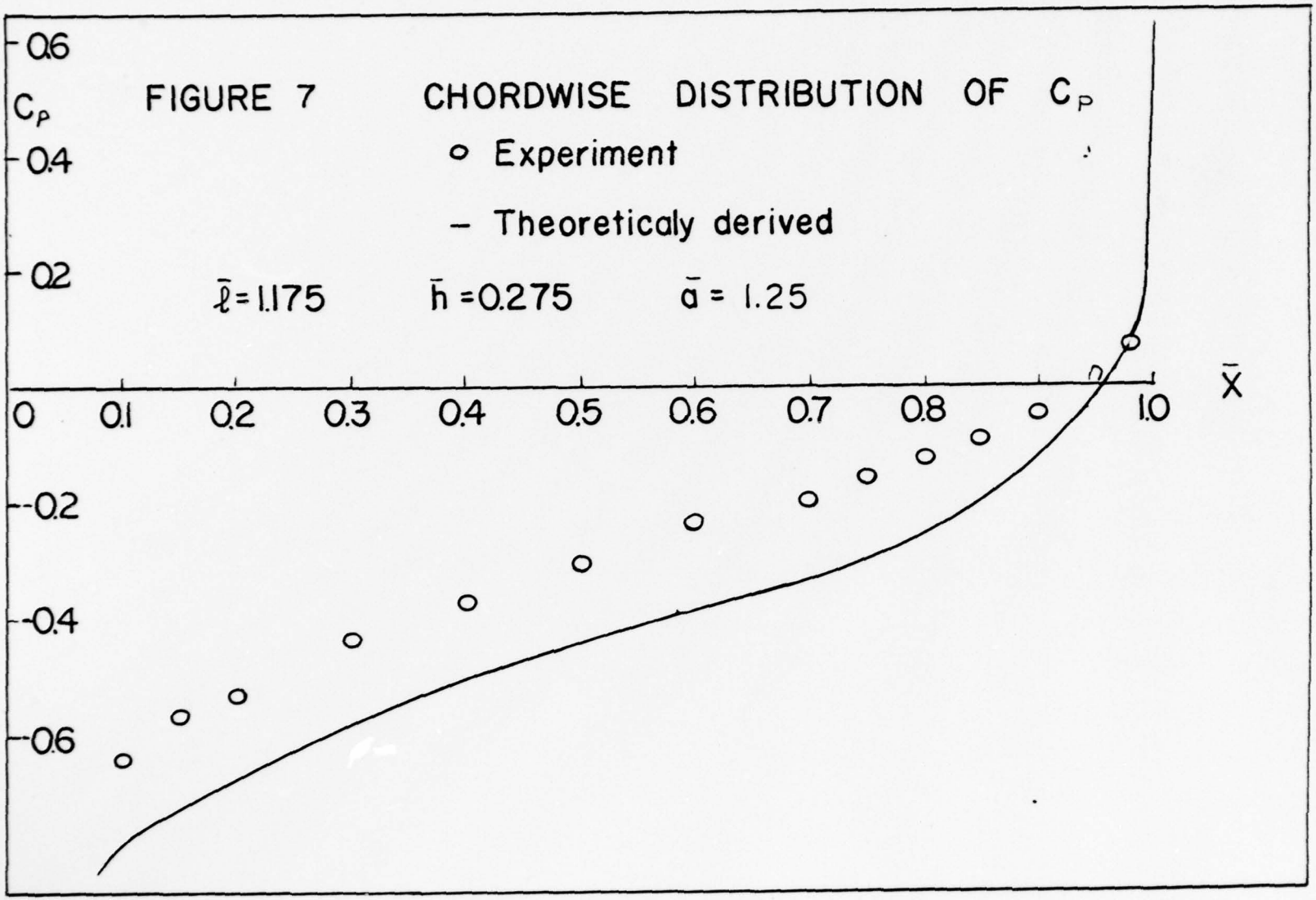
0.6
C_p
0.4
0.2
FIGURE 7 CHORDWISE DISTRIBUTION OF C_p
o Experiment
– Theoreticaly derived
$\bar{\ell}$=1.175 $\bar{h}$=0.275 $\bar{a}$ = 1.25
0 0.1 0.2 0.3 0.4 0.5 0.6 0.7 0.8 1.0
$\bar{X}$
-0.2
-0.4
-0.6

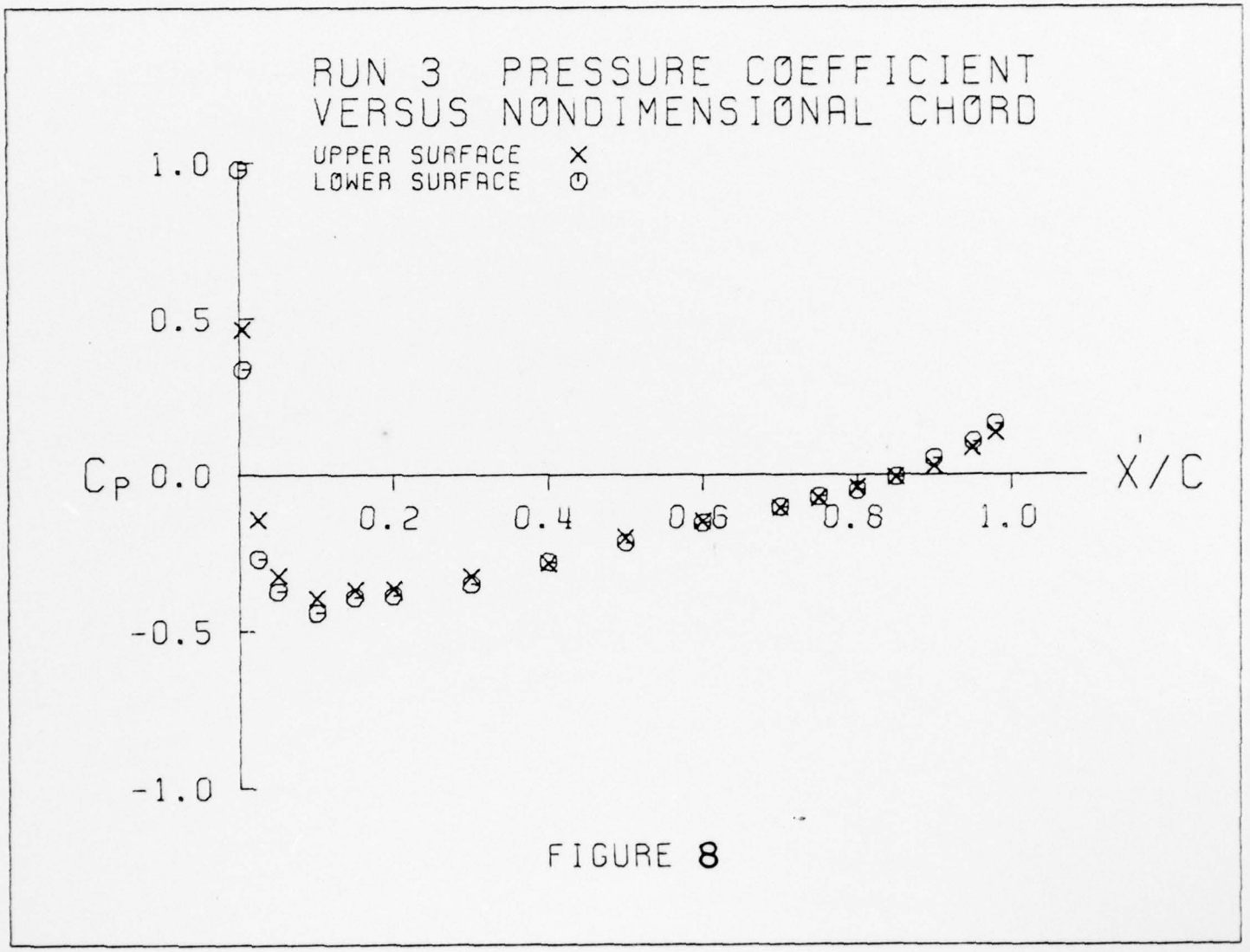
RUN 3 PRESSURE COEFFICIENT
VERSUS NONDIMENSIONAL CHORD
UPPER SURFACE
LOWER SURFACE
1.0
0.5
C_P 0.0
-0.5
-1.0
0.2
0.4
0.6
0.8
1.0
X'/C

FIGURE 8

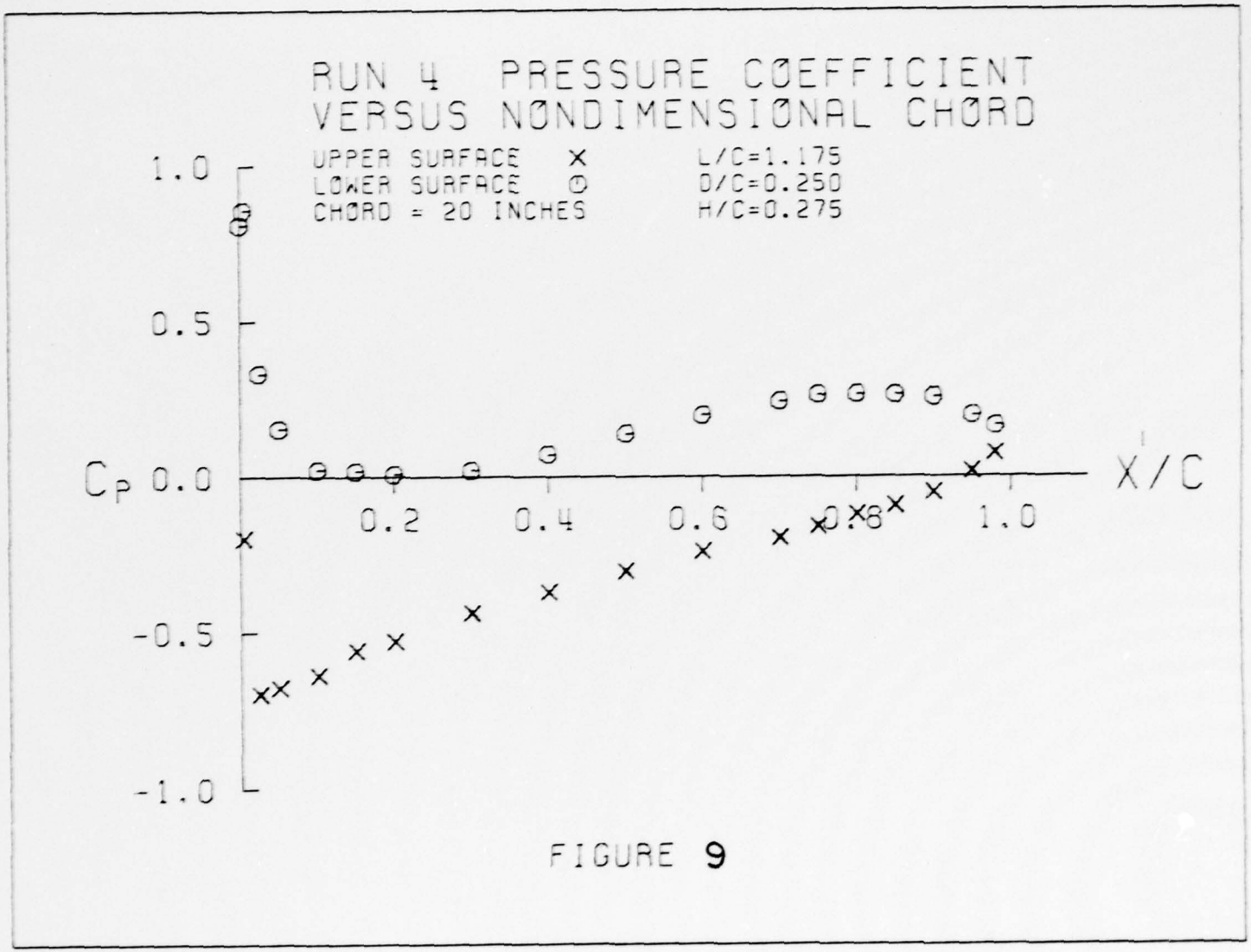
RUN 4 PRESSURE COEFFICIENT
VERSUS NONDIMENSIONAL CHORD
UPPER SURFACE X
LOWER SURFACE ⊙
CHORD = 20 INCHES
L/C=1.175
D/C=0.250
H/C=0.275
1.0
0.5
0.0
-0.5
-1.0
Cp
X/C
0.2
0.4
0.6
0.8
1.0

FIGURE 9

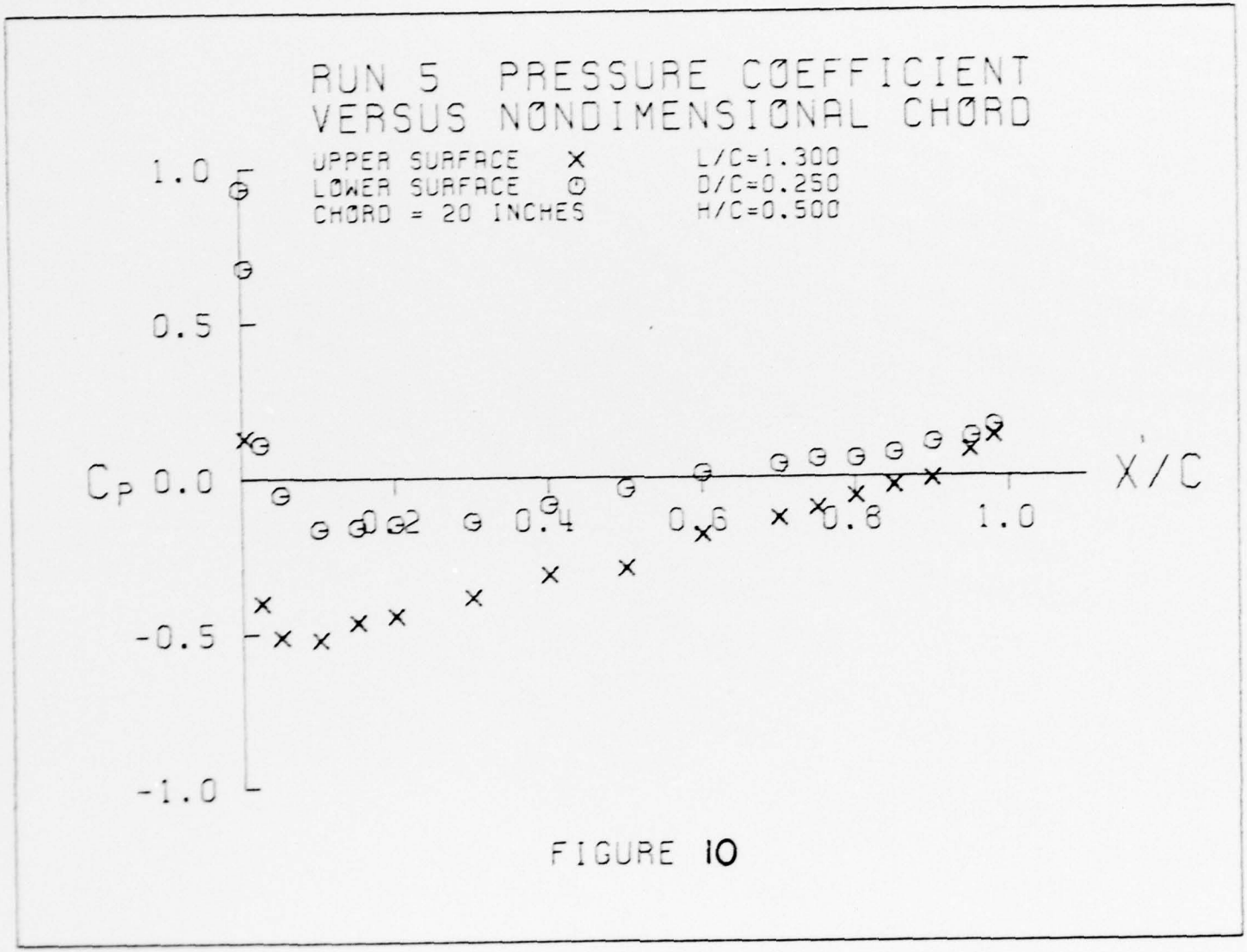
RUN 5 PRESSURE COEFFICIENT
VERSUS NONDIMENSIONAL CHORD
UPPER SURFACE X
LOWER SURFACE ⊙
CHORD = 20 INCHES
L/C=1.300
D/C=0.250
H/C=0.500
1.0
0.5
0.0
-0.5
-1.0
C_P
X/C
0.2
0.4
0.6
0.8
1.0

FIGURE 10

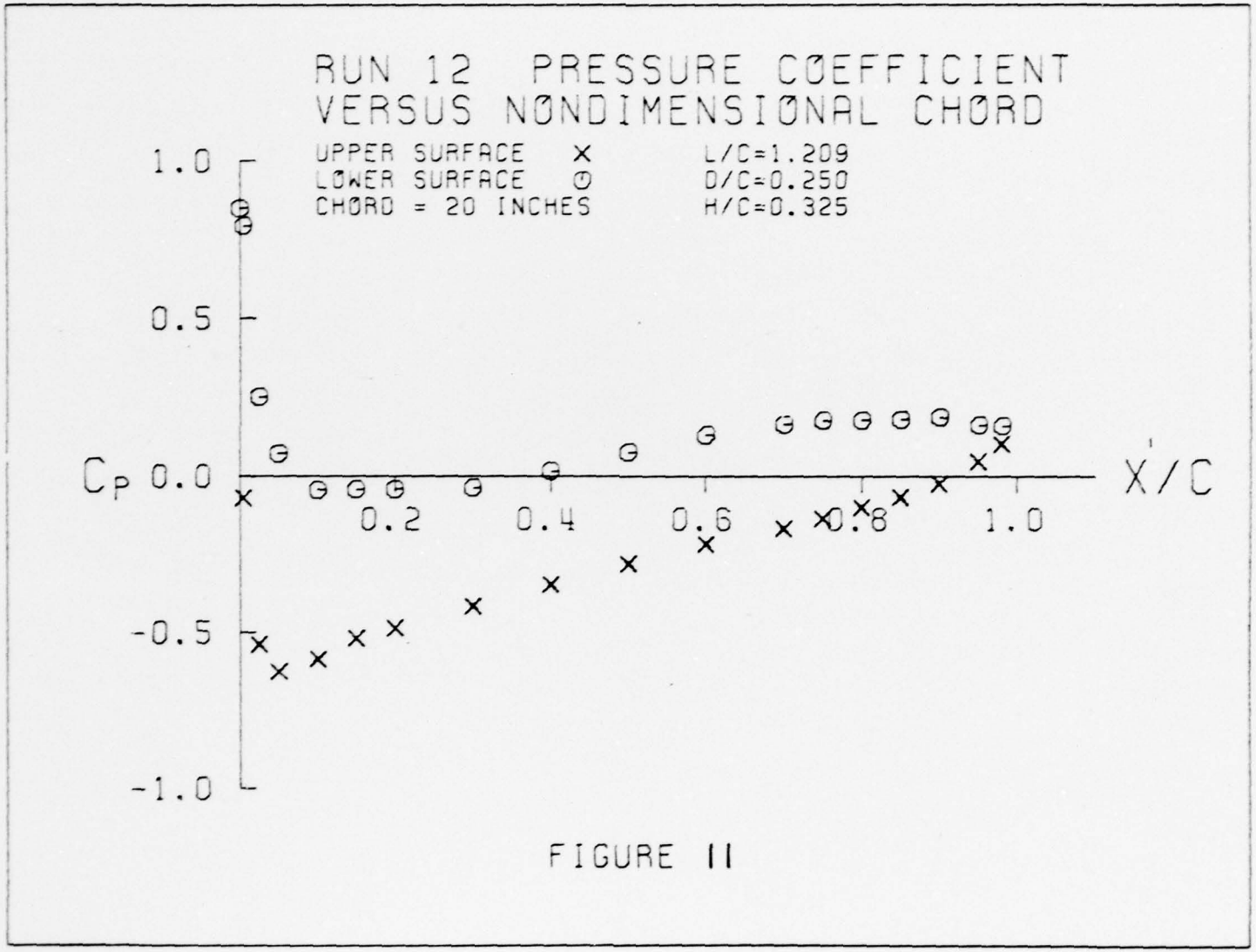
RUN 12 PRESSURE COEFFICIENT
VERSUS NONDIMENSIONAL CHORD
UPPER SURFACE X
LOWER SURFACE ⊙
CHORD = 20 INCHES
L/C=1.209
D/C=0.250
H/C=0.325
1.0
0.5
-0.5
-1.0
Cp 0.0
0.2
0.4
0.6
0.8
1.0
X/C

FIGURE 11

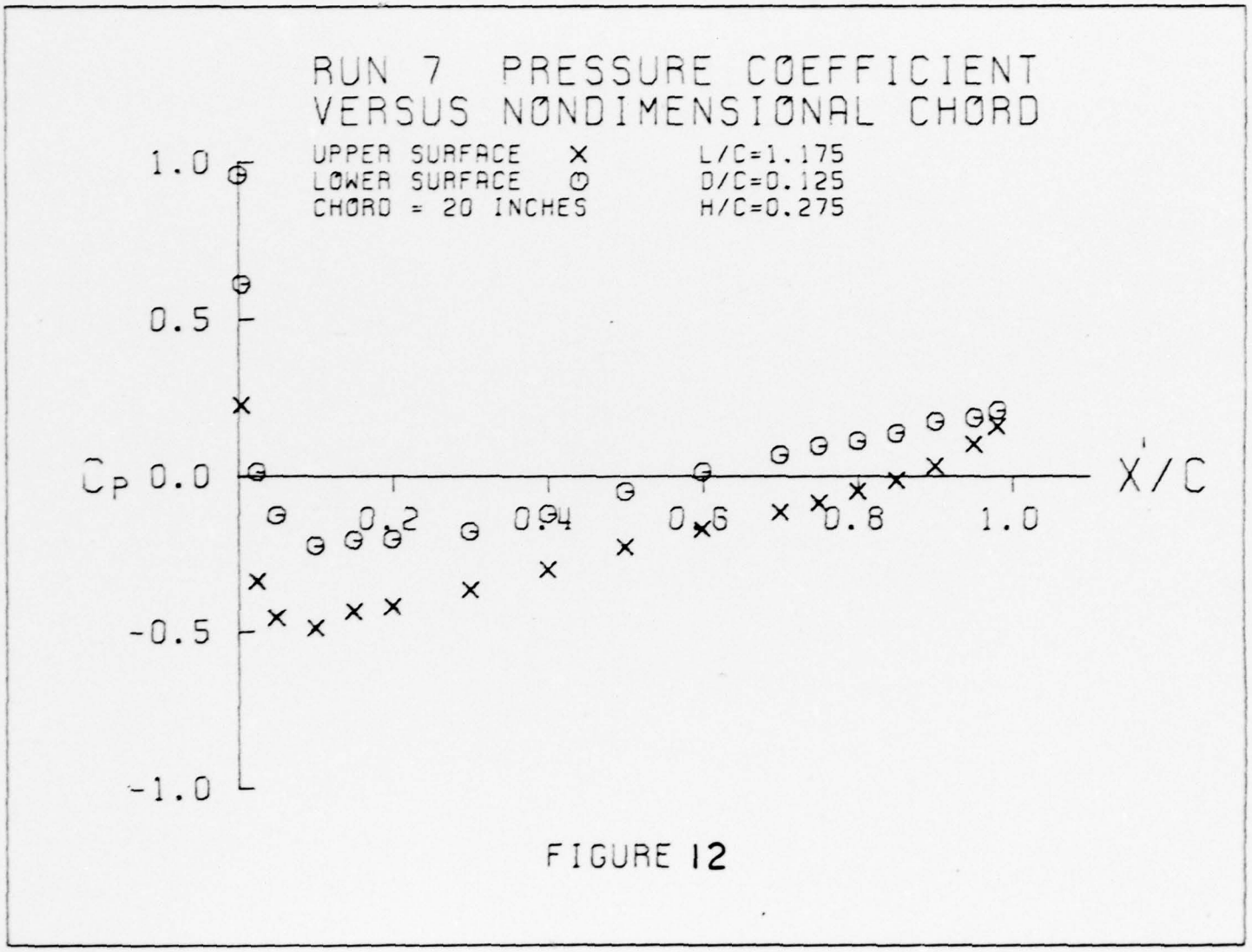
RUN 7 PRESSURE COEFFICIENT
VERSUS NONDIMENSIONAL CHORD
UPPER SURFACE X
LOWER SURFACE ⊙
CHORD = 20 INCHES
L/C=1.175
D/C=0.125
H/C=0.275
1.0
0.5
0.0
-0.5
-1.0
C_P
X/C
0.2
0.4
0.6
0.8
1.0

FIGURE 12

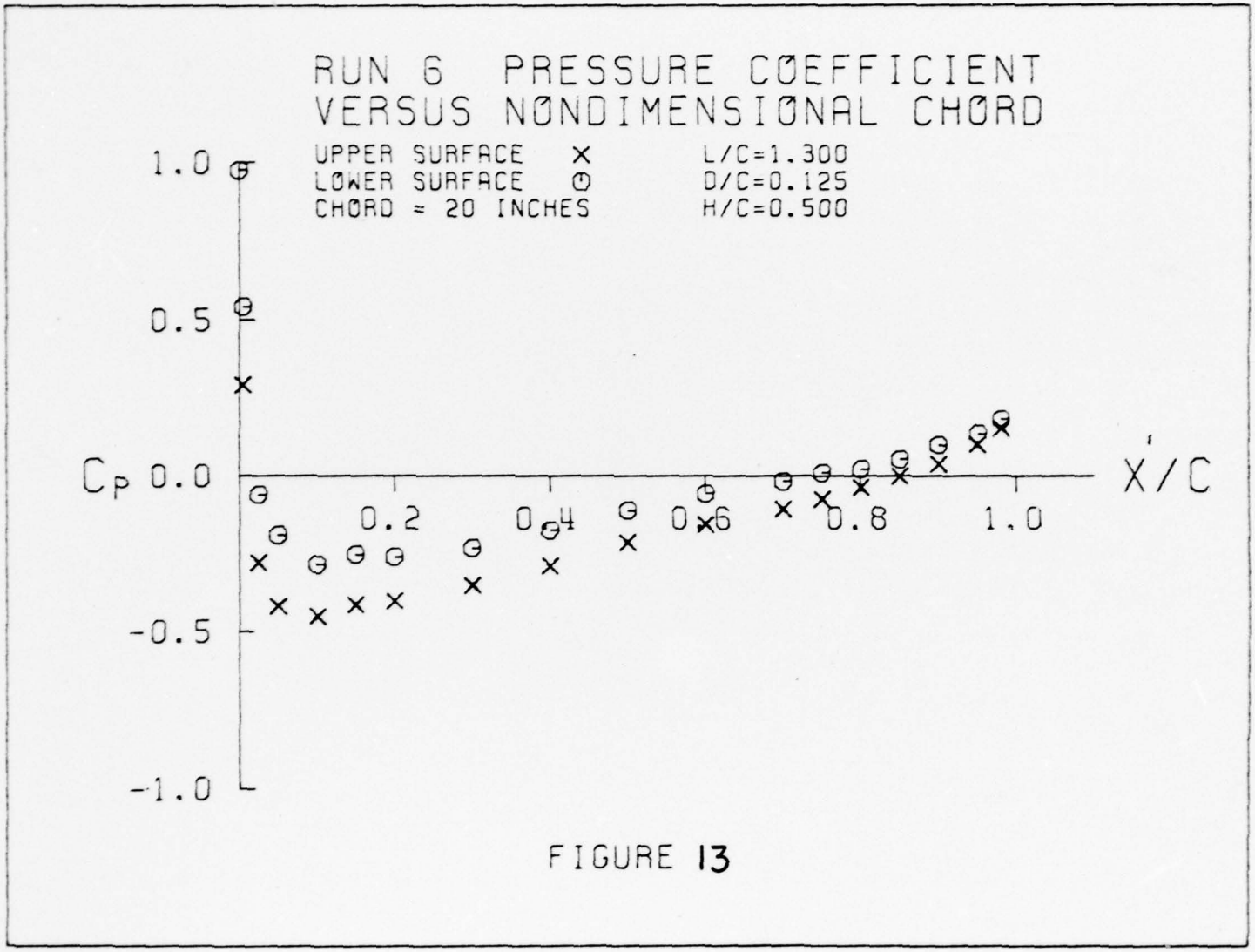
RUN 6 PRESSURE COEFFICIENT
VERSUS NONDIMENSIONAL CHORD
UPPER SURFACE
LOWER SURFACE
CHORD = 20 INCHES
L/C=1.300
D/C=0.125
H/C=0.500
1.0
0.5
0.0
-0.5
-1.0
C_P
X/C
0.2
0.4
0.6
0.8
1.0

FIGURE 13

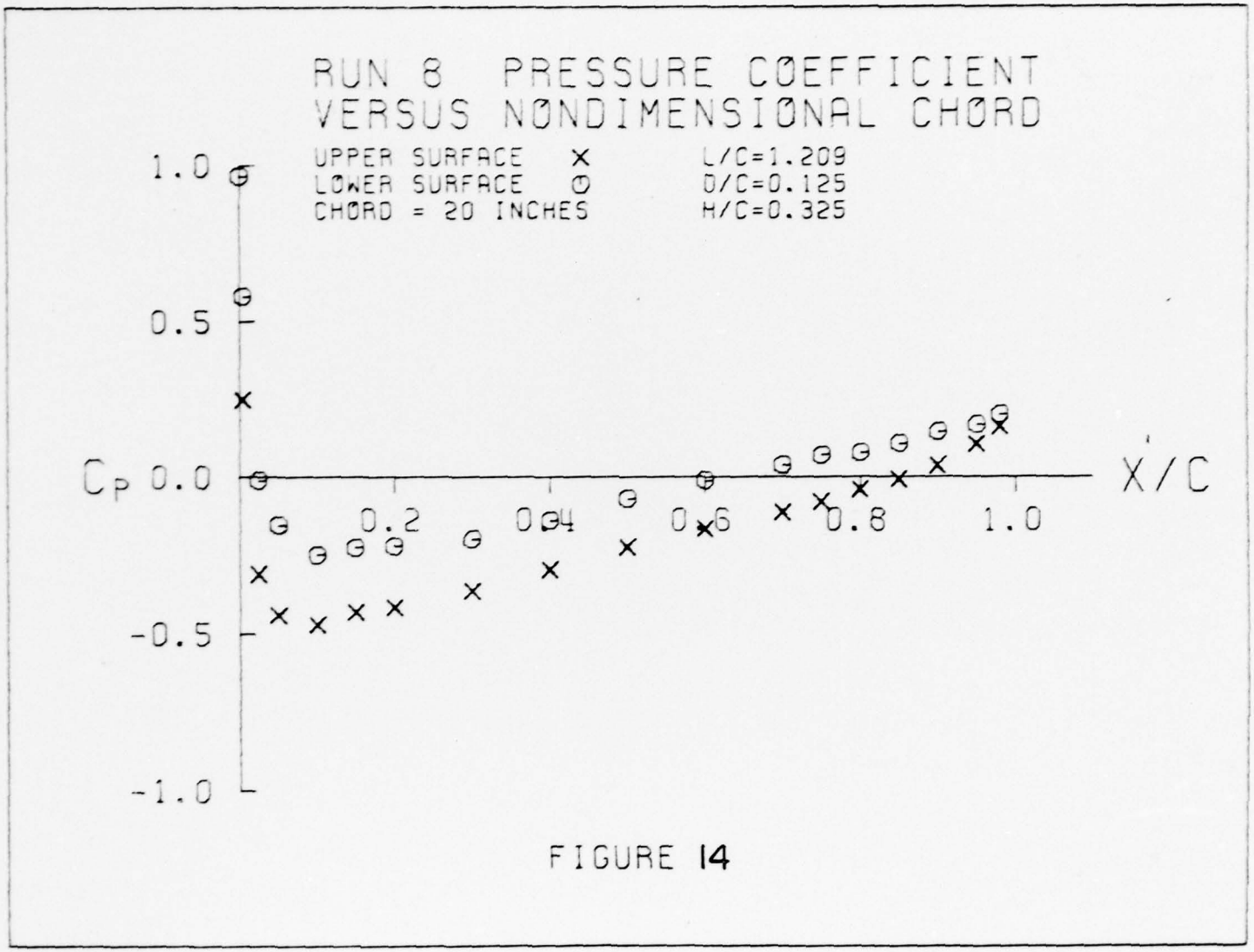
RUN 8 PRESSURE COEFFICIENT
VERSUS NONDIMENSIONAL CHORD
UPPER SURFACE X
LOWER SURFACE O
CHORD = 20 INCHES
L/C=1.209
D/C=0.125
H/C=0.325
1.0
0.5
-0.5
-1.0
Cp 0.0
0.2
0.4
0.6
0.8
1.0
X/C

FIGURE 14

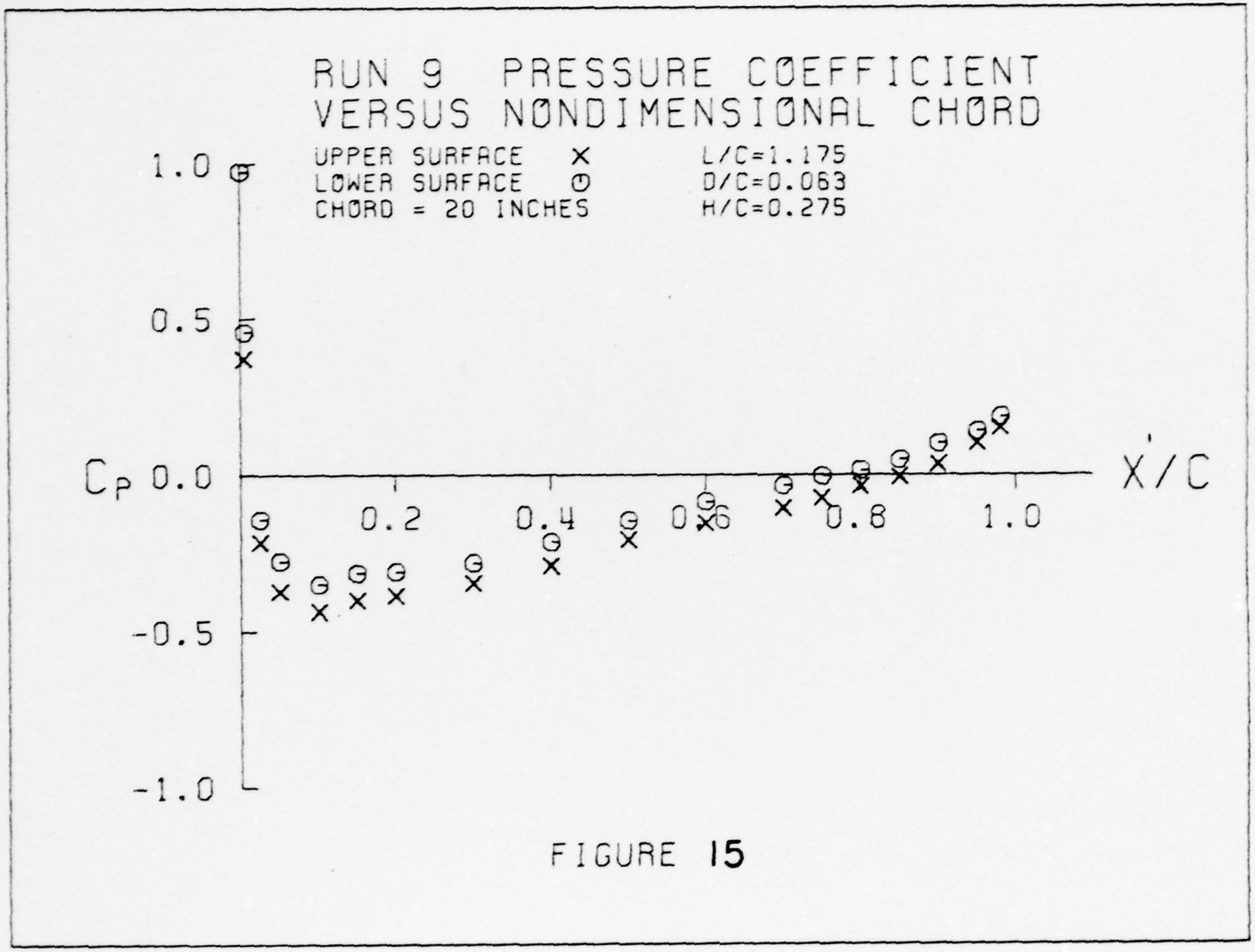
RUN 9 PRESSURE COEFFICIENT
VERSUS NONDIMENSIONAL CHORD
UPPER SURFACE X
LOWER SURFACE O
CHORD = 20 INCHES
L/C=1.175
D/C=0.063
H/C=0.275
1.0
0.5
Cp 0.0
-0.5
-1.0
0.2
0.4
0.6
0.8
1.0
X'/C

FIGURE 15

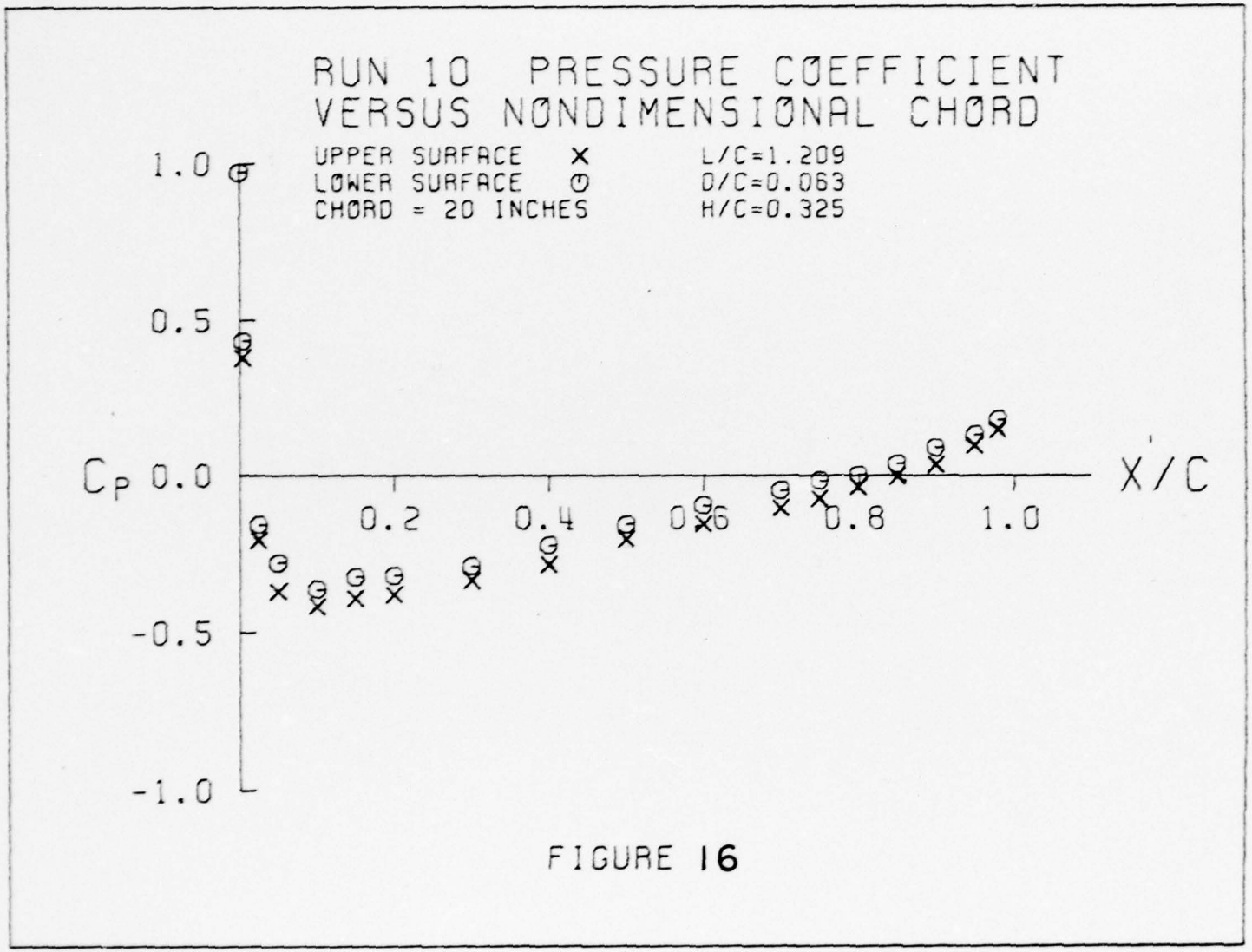
RUN 10 PRESSURE COEFFICIENT
VERSUS NONDIMENSIONAL CHORD
UPPER SURFACE ×
LOWER SURFACE ⊙
CHORD = 20 INCHES
L/C=1.209
D/C=0.063
H/C=0.325
1.0
0.5
C_P 0.0
-0.5
-1.0
0.2
0.4
0.6
0.8
1.0
X/C

FIGURE 16

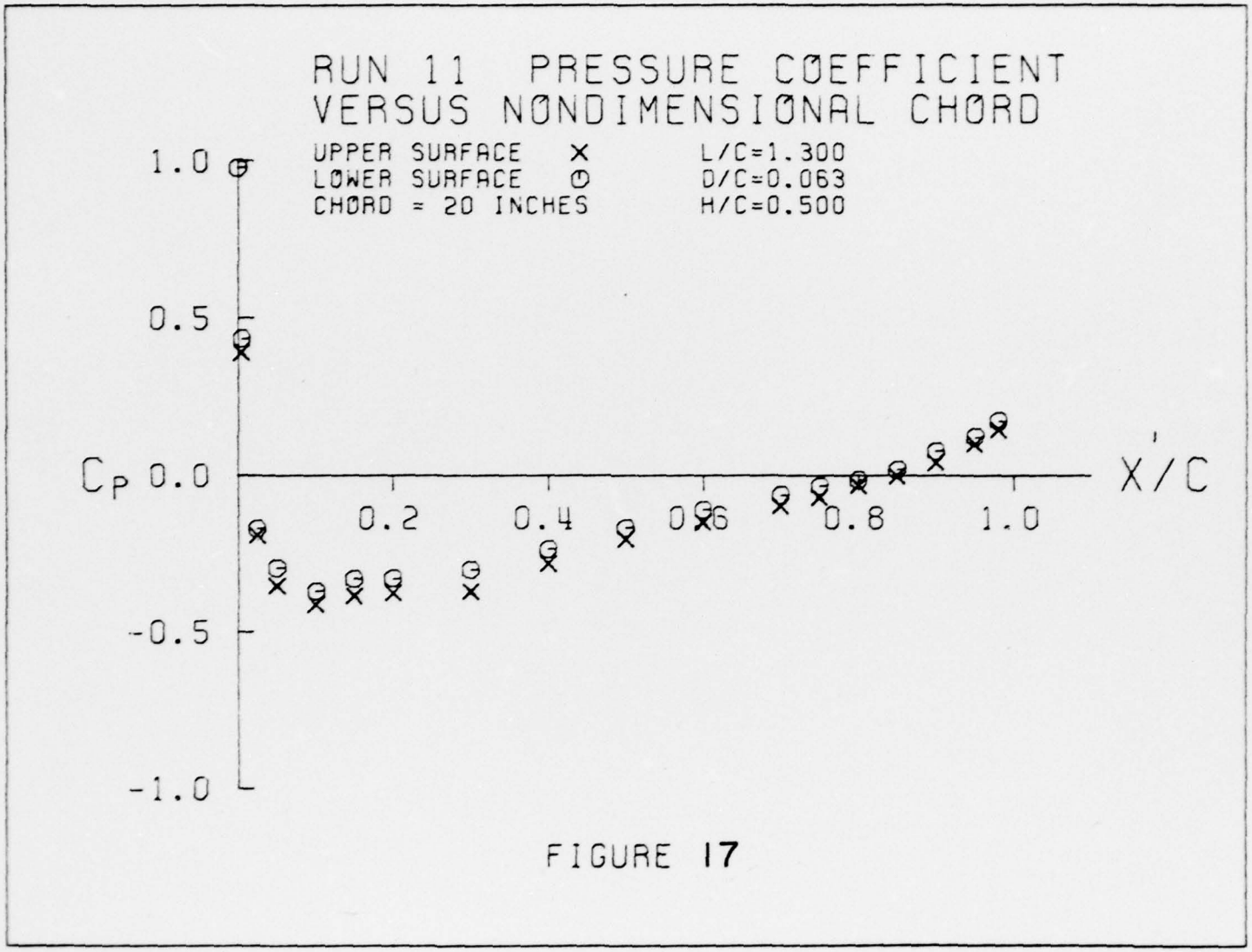
RUN 11 PRESSURE COEFFICIENT
VERSUS NONDIMENSIONAL CHORD
UPPER SURFACE X
LOWER SURFACE O
CHORD = 20 INCHES
L/C=1.300
D/C=0.063
H/C=0.500
1.0
0.5
0.0
-0.5
-1.0
Cp
0.2
0.4
0.6
0.8
1.0
X'/C

FIGURE 17

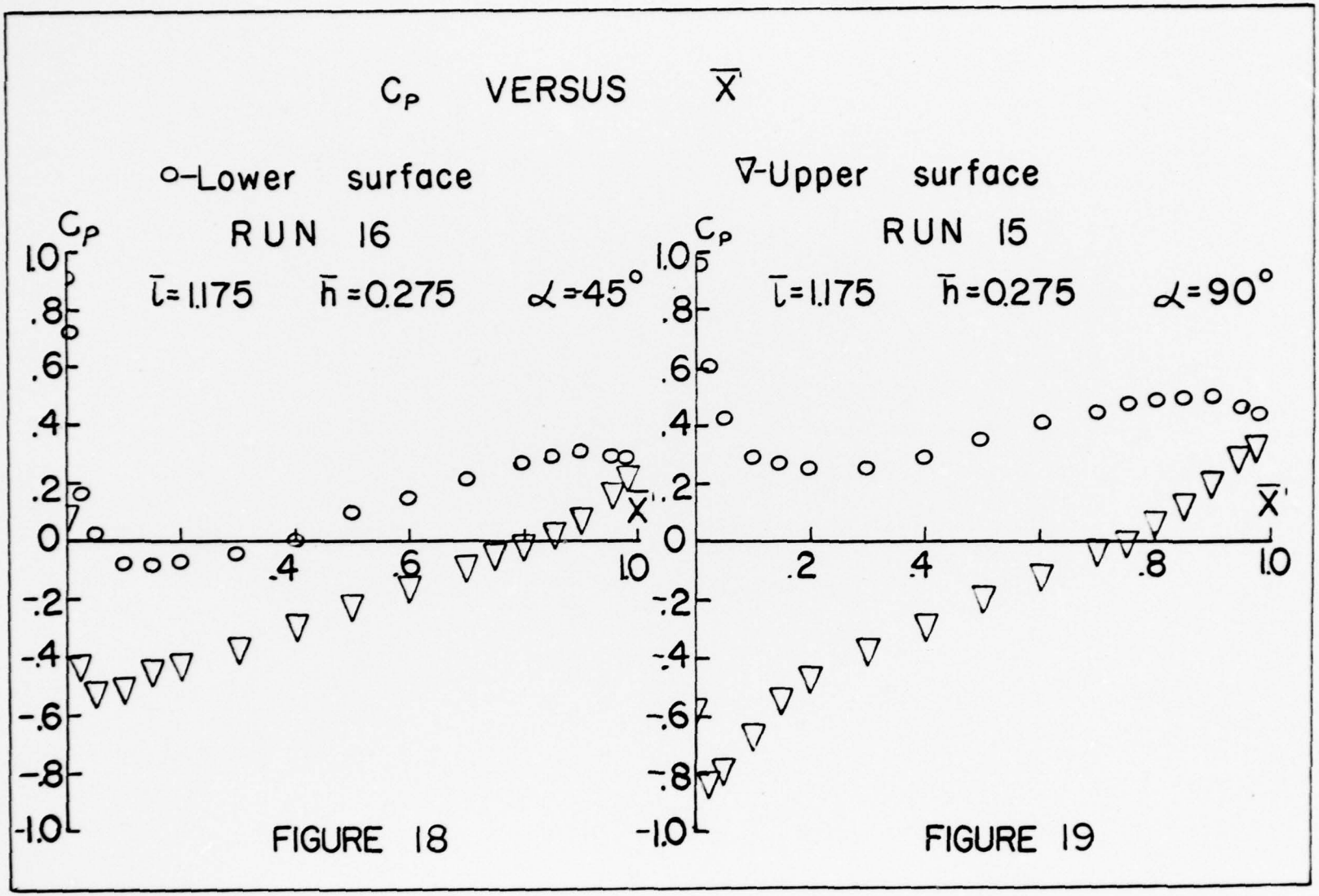

FIGURE 18

FIGURE 19

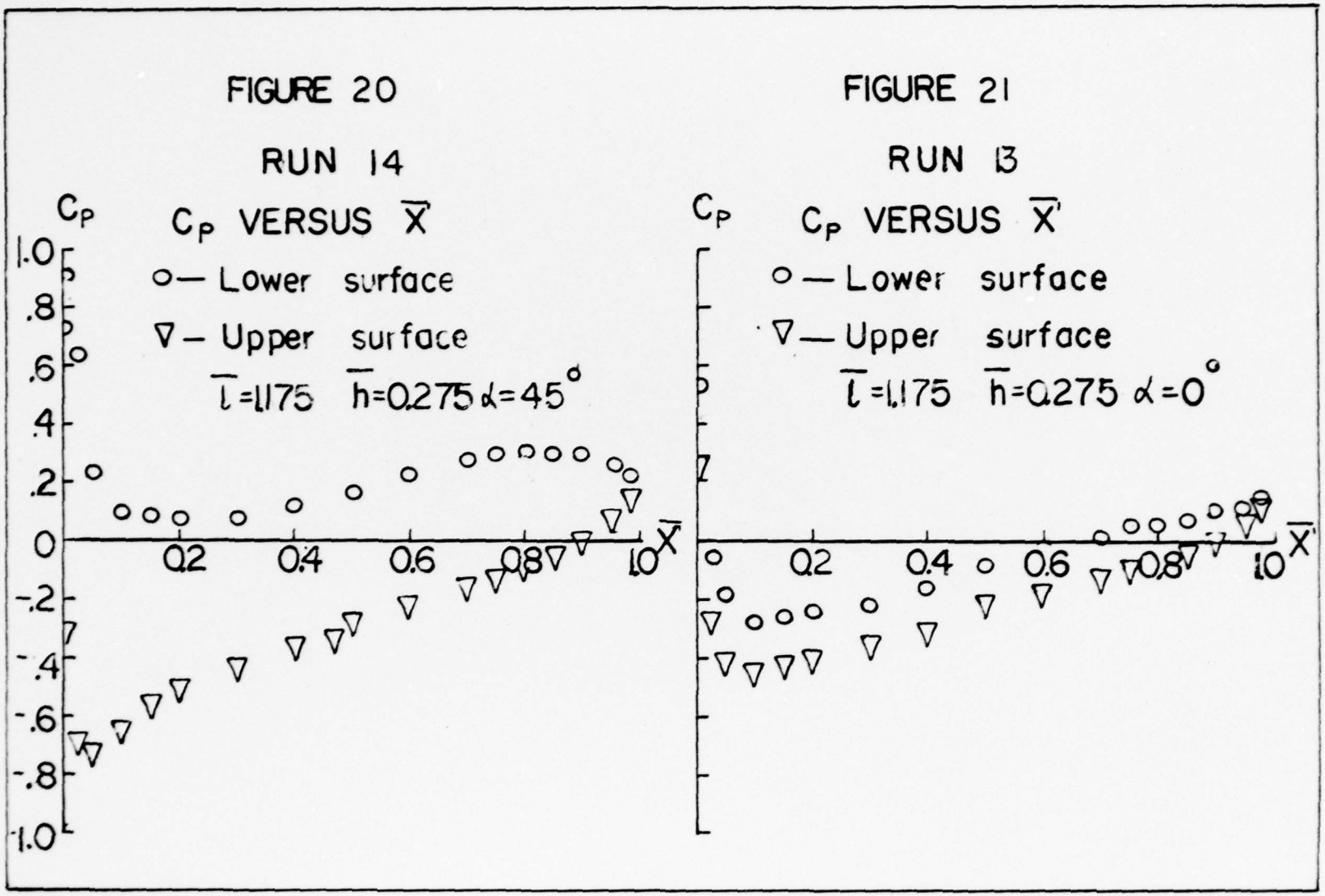
FIGURE 20
RUN 14
C_P VERSUS $\bar{X}$
C_P
o — Lower surface
∇ — Upper surface
$\bar{t}$=.175 $\bar{h}$=0.275 α=45°
1.0
.8
.6
.4
.2
0
-.2
-.4
-.6
-.8
-1.0
0.2
0.4
0.6
0.8
1.0
$\bar{X}$

FIGURE 21
RUN 13
C_P VERSUS $\bar{X}$
C_P
o — Lower surface
∇ — Upper surface
$\bar{t}$=.175 $\bar{h}$=0.275 α=0°
0.2
0.4
0.6
0.8
1.0
$\bar{X}$

References

1. Kenny, R B, ed, Proceedings of a Symposium on Unsteady Aerodynamics, University of Arizona, March, 1975.

2. Unsteady Air Loads in Separated and Transonic Flow, AGARD Conference Proceeding No. 226, July, 1977.

3. Kanevsky, A R, Comparison of Pressure Distribution Developed by Trailing Edge Flow Perturbation, S.M. Thesis, MIT, Dept of Aeronautics and Astronautics, Feb., 1978.

4. Schlicting, H, Boundary Layer Theory, Pergamon Press, New York, 1955, pp 465-471.

5. Duncan, W J, A S Thom and A D Young, Mechanics of Fluids, American Elisener Corp., New York, 1970.

6. Clauser, F H, Turbulent Boundary Layers in Adverse Pressure Gradients, Journal of the Aeronautical Sciences, Feb., 1954, pp 91-108.

7. Vagt, J D and H H Fernholz, Wall Interference Effects of Static Pressure Probes in an Incompressible Turbulent Boundary Layer, Aeronautical Quarterly, Vol XXVIII, Part 3, Aug., 1977, pp 176-184.

8. Abott, I H, and A E von Doenhoff, Theory of Wing Sections, Dover, New York.

9. Thwaites, B, Incompressible Aerodynamics, Claredon Press, Oxford, 1960, pp 120-125.

Appendix A

Schedule of Test Runs

The following is a list of the data measured during the test program. Several runs were eliminated when various errors in the measurements were discovered. For convenience, the wing data has been listed together with cylinder combination and wing ellipse combination.

Wing Cylinder Data

Run Number	$\bar{\ell}$	$\bar{h}$	$\bar{d}$	α^{o} ellipse
1	-	-	-	-
2	-	-	-	-
3	-	-	-	-
4	1.175	0.275	0.250	-
5	1.300	0.500	0.250	-
6	1.300	0.500	0.125	-
7	1.175	0.275	0.125	-
8	1.209	0.325	0.125	-
9	1.175	0.275	0.063	-
10	1.209	0.325	0.063	-
11	1.300	0.500	0.063	-
12	1.209	0.325	0.250	-
13	1.175	0.275	-	0
14	1.175	0.275	-	45
15	1.175	0.275	-	90
16	1.175	0.275	-	-45
17	1.175	0.275	-	22.5
18	1.175	0.275	-	67.5
25	1.300	0.500	-	0
26	1.300	0.500	-	22.5
27	1.300	0.500	-	45
28	1.300	0.500	-	-45
29	1.300	0.500	-	67.5
30	1.300	0.500	-	90